



occlusion level. Moreover, BOR calculations heavily rely on the union area of the occluder and the occludee, neglecting the area in which the object is occluded, which further reduces its utility in occlusion measurement. To this end, although labour-intensive, we choose a direct approach and manually label the observed occlusion level (low, mid, and high), resulting in a new dataset named COCO-OLAC, as shown in Fig. 2. We then investigate the performance of recent SOTA methods [24]–[29] in understanding occluded images by exploring their performance in the challenging image understanding task, i.e., panoptic segmentation, on the proposed COCO-OLAC dataset. Note that although this work explores the proposed benchmark on a panoptic segmentation task, the proposed occlusion benchmark can be utilised to aid any image understanding tasks such as object detection and image recognition. Building on this, we further evaluate the newly trained Mask2Former [28] across different occlusion levels. The experimental results show that performance decreases significantly as the occlusion level increases from low to high, underscoring the challenge that occlusion poses to SOTA panoptic segmentation methods.

As a first attempt to leverage the proposed occlusion annotations, we also propose a contrastive learning-based method to improve the representation learning of panoptic segmentation. Specifically, we utilise a triplet loss to bring samples having the same occlusion level closer in the feature space, while pushing apart samples with differing levels. Experiments show that the proposed method achieves state-of-the-art performance on the COCO-OLAC dataset. The ablation study further proves the effectiveness of the proposed method.

In summary, our contributions are three-fold:

- We establish and release a large-scale dataset, COCO-OLAC, which aims to aid occluded image understanding tasks. This dataset is derived from the COCO dataset by manually annotating the observed occlusion level, resulting in 30,000 training images and 5,000 test images.
- We systematically investigate the influence of the occlusion level by exploring the performance of SOTA panoptic segmentation methods in understanding the occluded images on the proposed benchmark.
- We devise a method to leverage the proposed occlusion annotations using contrastive learning to improve the representation learning for the panoptic segmentation task. The experimental results demonstrate the effectiveness of the proposed method.

## II. METHOD

### A. COCO-OLAC Dataset

a) *Dataset Annotation:* We annotate the occlusion levels of the images by the following three steps. For all the selected images, we first overlay polygon masks according to the ground truth annotation, since polygon masks can more accurately delineate the area of objects compared to bounding boxes. Then, we calculate the ratio of the occluded region to the entire occludee (including the occluded part), which is termed the occlusion rate. However, we cannot obtain the area

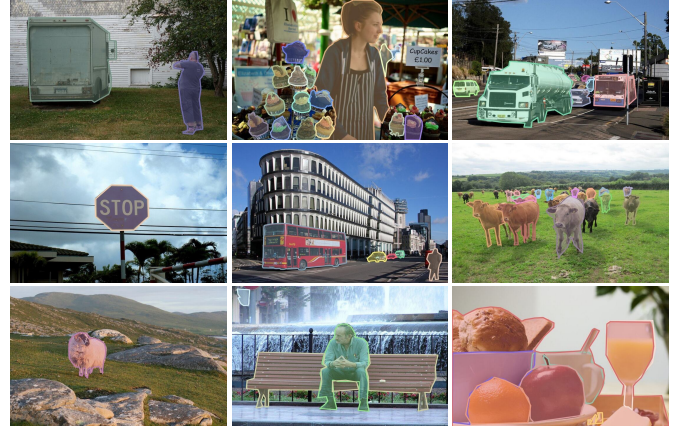


Fig. 2. Comparison of sample images with different occlusion levels from COCO-OLAC dataset. All images are overlaid with ground truth annotations to better show the occlusion relationship. The left, mid, and right columns show sample images with low, mid, and high occlusion levels, respectively. It is important to mention that only annotated instances are taken into account for assessment of the occlusion level.

of the occluded region directly because the COCO annotation only provides masks for visible parts of the objects. To resolve this issue, we have referred to a theory suggesting that people can estimate the shape of the occluded part of an object based on its overall shape, category, or relationship with other objects [41]. Therefore, we opt to visually estimate the shape of the occluded region and thereby estimate the occlusion rate of the occludee. Finally, the highest occlusion rate is defined as the occlusion level of the image. Based on this criterion, we manually classify the images into three occlusion levels: low, mid, and high, corresponding to the occlusion rate of  $[0\%, (0\%, 50\%]$  and  $(50\%, 100\%]$ , respectively. If the occlusion rate is difficult to estimate, which is often the case when determining the 50% threshold, we classify such images as having a mid occlusion level.

b) *Dataset Statistic:* The COCO-OLAC dataset contains 35k images, with 30k training images selected from the original COCO train2017 (first 30k images) and 5k val2017 images, which are the same as the original COCO validation set. For the training set, 12,081 images are annotated as high occlusion, 11,251 images as mid occlusion, and 6,668 images as low occlusion. For the validation set, 1,791 images are annotated as high occlusion, 2,075 images as mid occlusion, and 1,134 images as low occlusion. In addition, we separate the validation set into three subsets according to the occlusion level for further experimental validation of the models.

### B. Contrastive Learning on Occlusion Level

Having the annotation of the occlusion level on hand, we aim to leverage this information to improve the model performance on occluded image understanding. The model is expected to recognize the different occlusion levels from different images, so as to learn a more robust feature representation. One simplest way is to form a classification task based on the occlusion level. However, the classification requires samples from the same occlusion level to be strictly mapped into the same latent space, ignoring the similarities among

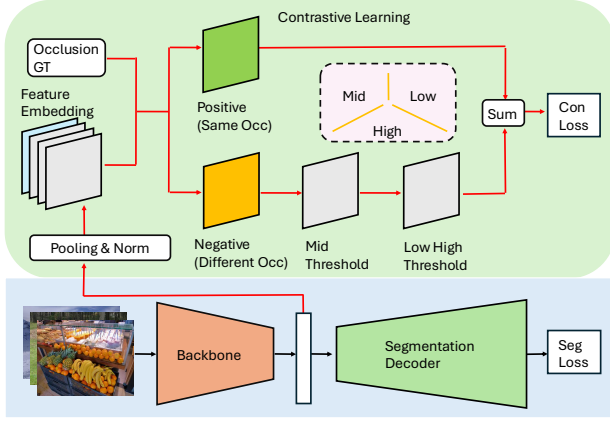


Fig. 3. The illustration of overall approach. The blue area below represents the schematic diagram of segmentation baseline, while the green area above illustrates our proposed contrastive learning-based method.

samples from different occlusion levels as the occlusion is a high-level concept. To this end, we employ a relatively soft method, the contrastive learning method, on the high-level image understanding task, i.e., panoptic segmentation, to improve the feature representation learning on occlusion. Specifically, we regard image pairs with the same occlusion level as positive pairs and those with different occlusion levels as negative pairs. A distance-based triplet loss is adopted to implement contrastive learning which could tolerate some dissimilarities between negative pairs.

The overall architecture is illustrated in Figure 3. In particular, we first feed the feature maps from the final layer of the backbone through  $Norm(AvgPool(X))$  to obtain the feature embeddings  $\tilde{z}$ . Then we calculate the cosine similarity by the function  $Sim(\cdot)$  based on  $\tilde{z}$  between image samples within a batch and apply the triplet loss as shown in Equation 1 to enable contrastive learning. Where  $y_i$  denotes the occlusion label for the  $i^{th}$  sample and  $\tau$  is the margin.

$$L_{con} = \frac{1}{B^2} \sum_{i=1}^B \left[ \sum_{j: y_j^d = y_i^d}^B (1 - Sim(\tilde{z}_i, \tilde{z}_j)) + \sum_{j: y_j^d \neq y_i^d}^B \max(0, Sim(\tilde{z}_i, \tilde{z}_j) - \tau) \right] \quad (1)$$

We observe a noticeable difference between images with low and high occlusion levels. In contrast, images with mid occlusion levels share more similarities with those at low or high occlusion levels in the occlusion space. Given this, we propose to set two margins for the low-high image pairs and other pairs, respectively. Specifically, we set a strict threshold  $\tau_{l,h}$  to push low-high image pairs closer and a higher threshold  $\tau_m$  for other pairs to tolerate more dissimilarity.

Through the proposed contrastive learning, the model can capture the occlusion difference from different samples, thus learning a more discriminative and robust feature representation. The model is jointly optimised by the proposed contrastive loss  $L_{con}$  and the panoptic segmentation loss  $L_{seg}$ . The

TABLE I  
SOTA PERFORMANCE ON DIFFERENT OCCLUSION LEVELS.

Method	Occlusion	PQ	PQ <sup>Th</sup>	PQ <sup>St</sup>	AP <sup>Th</sup> <sub>pan</sub>	mIoU <sub>pan</sub>
Panoptic FPN [24]	low	43.8	53.2	29.5	-	-
	mid	40.2	47.3	29.5	-	-
	high	34.5	39.0	27.7	-	-
Panoptic FCN [25]	low	46.9	56.1	33.3	-	-
	mid	41.9	48.2	32.5	-	-
	high	36.3	40.4	30.1	-	-
Panoptic DeepLab [26]	low	42.9	47.8	35.5	-	-
	mid	36.2	39.4	31.3	-	-
	high	30.3	31.0	29.2	-	-
MaskFormer [27]	low	52.6	58.8	43.3	-	-
	mid	48.0	53.9	39.1	-	-
	high	41.2	44.0	37.0	-	-
Mask2Former [28]	low	56.8	64.4	45.8	56.5	60.4
	mid	53.3	60.1	43.0	45.1	61.2
	high	46.7	51.3	39.7	35.8	58.1
Mask DINO [29]	low	56.6	63.1	47.0	56.4	58.0
	mid	53.7	60.6	43.4	47.2	59.7
	high	48.3	53.3	40.8	38.8	57.4

TABLE II  
COMPARISON OF SOTA PANOPTIC SEGMENTATION METHODS ON THE COCO-OLAC DATASET VIA RETRAINING ON COCO-OLAC DATASET.

Model	PQ	PQ <sup>Th</sup>	PQ <sup>St</sup>	AP <sup>Th</sup> <sub>pan</sub>	mIoU <sub>pan</sub>
Panoptic FPN [24]	33.3	39.1	24.6	-	-
Panoptic-DeepLab [26]	27.5	28.9	25.3	-	-
Panoptic FCN [25]	33.0	37.7	26.0	-	-
Mask2Former [28]	41.5	45.3	35.6	30.6	<b>54.4</b>
YOSO [30]	37.1	40.6	31.9	-	-
Ours	<b>41.8</b>	<b>45.3</b>	<b>36.4</b>	<b>30.8</b>	54.3

final loss  $L_{fin}$  is shown in Equation 2 where  $\lambda$  is a hyperparameter to balance the contribution between segmentation and contrastive learning.

$$L_{fin} = L_{seg} + \lambda L_{con} \quad (2)$$

### III. EXPERIMENTS

We investigate how images with different occlusion levels affect the performance of the SOTA panoptic segmentation method using the newly proposed COCO-OLAC dataset. Apart from the standard panoptic segmentation metric PQ [23], we also report AP<sup>Th</sup><sub>pan</sub> and mIoU<sub>pan</sub> [28] for instance segmentation and semantic segmentation, respectively. Finally, we demonstrate the effectiveness of our proposed methods through ablation studies.

#### A. Implementation Details

For experiments investigating the influence of different occlusion levels, we conduct a validation experiment that loads the pre-trained weights (trained on the entire COCO dataset) of recent SOTA panoptic segmentation methods and tests their performance on the different validation subsets (occlusion level) of the proposed COCO-OLAC using the official code and scripts. For experiments verifying the effectiveness of our proposed method, we adopt Mask2Former (with ResNet-50) as our baseline and train the model on the training set of our proposed COCO-OLAC dataset. All the compared methods on this experiment are reimplemented on the COCO-OLAC dataset using the official code. The input images are resized



TABLE III  
COMPARISON ACROSS LOW, MID, AND HIGH OCCLUSION LEVELS FOR PROPOSED METHODS AND BASELINE VIA RETRAINING.

Occlusion	Model	PQ	PQ <sup>Th</sup>	PQ <sup>St</sup>	AP <sup>Th</sup> <sub>pan</sub>	mIoU <sub>pan</sub>
low	base	47.5	<b>53.5</b>	38.5	<b>46.7</b>	52.2
	con	<b>48.1(+0.6)</b>	53.1	<b>40.8(+2.3)</b>	46.4	<b>52.7(+0.5)</b>
mid	base	43.1	<b>48.1</b>	35.6	33.3	<b>54.0</b>
	con	<b>43.2</b>	47.9	<b>36.1(+0.5)</b>	<b>33.7(+0.4)</b>	54.0
high	base	35.7	38.2	32.0	<b>24.8</b>	50.7
	con	<b>36.1(+0.4)</b>	<b>38.2</b>	<b>33.0(+1.0)</b>	24.7	<b>50.8</b>

TABLE IV  
ABLATION STUDY ON THE PROPOSED METHOD.

Model $\tau$	PQ	PQ <sup>Th</sup>	PQ <sup>St</sup>	AP <sup>Th</sup> <sub>pan</sub>	mIoU <sub>pan</sub>
Base	41.5	45.3	35.6	30.6	<b>54.4</b>
Our	<b>41.8(+0.3)</b>	<b>45.3</b>	<b>36.4(+0.8)</b>	<b>30.8</b>	54.3

and cropped into  $512 \times 512$ .  $\lambda$  in equation 2 is set to 1.0. The margins  $\tau_{l,h}$  and  $\tau_m$  are set to 0.4 and 0.6 respectively.

### B. Experimental Results

Herein, we first benchmark the performance of the SOTA panoptic segmentation methods, including Panoptic FPN [24], Panoptic DeepLab [26], Panoptic FCN [25], Mask2Former [28] and Mask DINO [29], on the proposed COCO-OLAC validation set. In particular, we report the results on different levels of occlusion (subsets), as shown in Table I. The results show a clear trend: As the level of occlusion increases from low to high, the performance metrics (PQ, PQ<sup>Th</sup>, PQ<sup>St</sup>, and AP<sup>Th</sup><sub>pan</sub>) experience a significant decline. This degradation highlights a critical limitation of current SOTA panoptic segmentation methods, which struggle to maintain accuracy and consistency in handling occlusion. Moreover, it also confirms the correctness of our manual annotation that reflects the level of occlusion of the image.

Then, we verify the effectiveness of our proposed method by retraining and testing the model on the COCO-OLAC. We demonstrate the results of our proposed method and the baseline on all three levels of occlusion subsets of the validation set in Table III and compare our method with recent SOTA methods in Table II. As can be seen, the model equipped with the proposed contrastive learning shows substantial improvements at all levels of occlusion. Specifically, for low occlusion, PQ improves by 0.6, and PQ<sup>St</sup> sees a notable increase of 2.3, indicating a strong improvement in the segmentation of 'stuff' classes. Similarly, under high occlusion, the method produces a 0.4 improvement in PQ and a 1.0 increase in PQ<sup>St</sup>. All results demonstrate the effectiveness of our method compared to the baseline in a range of occlusion levels. Note that the panoptic segmentation is a challenging task, especially on the large-scale challenging COCO dataset, where even a small improvement proves difficult. Moreover, our method obtains the best overall performance over previous SOTA methods. These results confirm our theory and demonstrate that the representation of the occlusion feature can assist in training and improve overall segmentation accuracy, especially in segmenting and labelling larger and less defined regions.

TABLE V  
IMPACT OF  $\tau_{l,h}$  AND  $\tau_m$  COMBINATIONS ON THE PERFORMANCE OF CONTRASTIVE LEARNING-BASED METHOD

$\tau_{l,h}$	$\tau_m$	PQ	PQ <sup>Th</sup>	PQ <sup>St</sup>
0.3	0.4	41.3	45.0	35.8
0.3	0.6	41.2	44.9	35.6
0.3	0.8	41.4	45.2	35.7
0.4	0.6	<b>41.8</b>	<b>45.3</b>	<b>36.4</b>
0.4	0.7	41.3	45.1	35.7

### C. Ablation Study

In addition to the ablation study in Table III, we further conduct an ablation study to analyse the effectiveness of our method on the entire validation set.

As shown in IV, after adding the proposed method, an improvement can be seen on both the various occlusion subsets and the entire validation set, especially PQ<sup>St</sup>, which improves by 0.8 on the entire validation set. This indicates that the proposed contrastive learning method enhances the model's ability to learn a more occlusion-robust feature, thereby improving its overall performance.

Then, we investigate the influence of the margins in our proposed contrastive learning method in Table V. In particular, we first evaluate the combination of thresholds of  $\tau_{l,h}$  and  $\tau_m$  by keeping one threshold fixed while increasing the other. When the first threshold  $\tau_{l,h}$  is fixed at 0.3, increasing the second threshold  $\tau_m$  (from 0.4 to 0.8) shows a minimal effect on overall performance. When  $\tau_{l,h}$  increases to 0.4, the combination of  $\tau_{l,h} = 0.4$  and  $\tau_m = 0.6$  achieves the highest PQ. However, with further increases of  $\tau_m$  beyond 0.6, the overall performance starts to decline. This trend demonstrates that neglecting the influence of either threshold will result in a degradation of overall performance.

Our method is the initial attempt to utilise the occlusion annotations. We believe that a more significant improvement can be achieved when further advanced methods are proposed to better optimise our proposed dataset.

## IV. CONCLUSION

In this work, we introduce COCO-OLAC, a novel large-scale dataset designed to facilitate research on occlusion in panoptic segmentation and other image understanding tasks. The dataset, derived from the COCO dataset with manual occlusion annotations, provides a comprehensive benchmark with over 30,000 training images and 5,000 test images categorised into three occlusion levels. Our experiments systematically evaluated the performance of SOTA panoptic segmentation methods on this dataset, revealing that occlusion, especially at higher levels, substantially degrades model performance. In addition, we propose a contrastive learning-based method to enhance model robustness in handling occlusion. Despite its simplicity, our approach yields performance improvements over the baseline. This work not only highlights the significant impact of occlusion on the panoptic segmentation task but also offers a quantitative foundation for future research into more effective occlusion-aware methods.

## REFERENCES

- [1] J. Deng, W. Dong, R. Socher, L.-J. Li, K. Li, and L. Fei-Fei, "Imagenet: A large-scale hierarchical image database," in *2009 IEEE conference on computer vision and pattern recognition*. Ieee, 2009, pp. 248–255.
- [2] B. Zhou, H. Zhao, X. Puig, S. Fidler, A. Barriuso, and A. Torralba, "Scene parsing through ade20k dataset," in *Proceedings of the IEEE conference on computer vision and pattern recognition*, 2017, pp. 633–641.
- [3] M. Cordts, M. Omran, S. Ramos, T. Rehfeld, M. Enzweiler, R. Benenson, U. Franke, S. Roth, and B. Schiele, "The cityscapes dataset for semantic urban scene understanding," in *Proceedings of the IEEE conference on computer vision and pattern recognition*, 2016, pp. 3213–3223.
- [4] T.-Y. Lin, M. Maire, S. Belongie, J. Hays, P. Perona, D. Ramanan, P. Dollár, and C. L. Zitnick, "Microsoft coco: Common objects in context," in *Computer Vision—ECCV 2014: 13th European Conference, Zurich, Switzerland, September 6–12, 2014, Proceedings, Part V 13*. Springer, 2014, pp. 740–755.
- [5] G. Neuhold, T. Ollmann, S. Rota Buló, and P. Kotschieder, "The mapillary vistas dataset for semantic understanding of street scenes," in *Proceedings of the IEEE international conference on computer vision*, 2017, pp. 4990–4999.
- [6] A. Geiger, P. Lenz, and R. Urtasun, "Are we ready for autonomous driving? the kitti vision benchmark suite," in *2012 IEEE conference on computer vision and pattern recognition*. IEEE, 2012, pp. 3354–3361.
- [7] R. Szeliski, *Computer vision: algorithms and applications*. Springer Nature, 2022.
- [8] S. Ren, K. He, R. Girshick, and J. Sun, "Faster r-cnn: Towards real-time object detection with region proposal networks," *IEEE transactions on pattern analysis and machine intelligence*, vol. 39, no. 6, pp. 1137–1149, 2016.
- [9] W. Liu, D. Anguelov, D. Erhan, C. Szegedy, S. Reed, C.-Y. Fu, and A. C. Berg, "Ssd: Single shot multibox detector," in *Computer Vision—ECCV 2016: 14th European Conference, Amsterdam, The Netherlands, October 11–14, 2016, Proceedings, Part I 14*. Springer, 2016, pp. 21–37.
- [10] T.-Y. Ross and G. Dollár, "Focal loss for dense object detection," in *proceedings of the IEEE conference on computer vision and pattern recognition*, 2017, pp. 2980–2988.
- [11] T.-Y. Lin, P. Dollár, R. Girshick, K. He, B. Hariharan, and S. Belongie, "Feature pyramid networks for object detection," in *Proceedings of the IEEE conference on computer vision and pattern recognition*, 2017, pp. 2117–2125.
- [12] Z. Cai and N. Vasconcelos, "Cascade r-cnn: Delving into high quality object detection," in *Proceedings of the IEEE conference on computer vision and pattern recognition*, 2018, pp. 6154–6162.
- [13] N. Carion, F. Massa, G. Synnaeve, N. Usunier, A. Kirillov, and S. Zagoruyko, "End-to-end object detection with transformers," in *European conference on computer vision*. Springer, 2020, pp. 213–229.
- [14] X. Zhu, W. Su, L. Lu, B. Li, X. Wang, and J. Dai, "Deformable detr: Deformable transformers for end-to-end object detection," *arXiv preprint arXiv:2010.04159*, 2020.
- [15] S. Liu, F. Li, H. Zhang, X. Yang, X. Qi, H. Su, J. Zhu, and L. Zhang, "Dab-detr: Dynamic anchor boxes are better queries for detr," *arXiv preprint arXiv:2201.12329*, 2022.
- [16] H. Zhang, F. Li, S. Liu, L. Zhang, H. Su, J. Zhu, L. M. Ni, and H.-Y. Shum, "Dino: Detr with improved denoising anchor boxes for end-to-end object detection," *arXiv preprint arXiv:2203.03605*, 2022.
- [17] A. Wang, H. Chen, L. Liu, K. Chen, Z. Lin, J. Han, and G. Ding, "Yolov10: Real-time end-to-end object detection," *arXiv preprint arXiv:2405.14458*, 2024.
- [18] K. He, G. Gkioxari, P. Dollár, and R. Girshick, "Mask r-cnn," in *Proceedings of the IEEE international conference on computer vision*, 2017, pp. 2961–2969.
- [19] S. Liu, L. Qi, H. Qin, J. Shi, and J. Jia, "Path aggregation network for instance segmentation," in *Proceedings of the IEEE conference on computer vision and pattern recognition*, 2018, pp. 8759–8768.
- [20] D. Bolya, C. Zhou, F. Xiao, and Y. J. Lee, "Yolact: Real-time instance segmentation," in *Proceedings of the IEEE/CVF international conference on computer vision*, 2019, pp. 9157–9166.
- [21] X. Wang, R. Zhang, T. Kong, L. Li, and C. Shen, "Solov2: Dynamic and fast instance segmentation," *Advances in Neural information processing systems*, vol. 33, pp. 17 721–17 732, 2020.
- [22] Y. Lee and J. Park, "Centermask: Real-time anchor-free instance segmentation," in *Proceedings of the IEEE/CVF conference on computer vision and pattern recognition*, 2020, pp. 13 906–13 915.
- [23] A. Kirillov, K. He, R. Girshick, C. Rother, and P. Dollár, "Panoptic segmentation," in *Proceedings of the IEEE/CVF conference on computer vision and pattern recognition*, 2019, pp. 9404–9413.
- [24] A. Kirillov, R. Girshick, K. He, and P. Dollár, "Panoptic feature pyramid networks," in *Proceedings of the IEEE/CVF conference on computer vision and pattern recognition*, 2019, pp. 6399–6408.
- [25] Y. Li, H. Zhao, X. Qi, L. Wang, Z. Li, J. Sun, and J. Jia, "Fully convolutional networks for panoptic segmentation," in *Proceedings of the IEEE/CVF conference on computer vision and pattern recognition*, 2021, pp. 214–223.
- [26] B. Cheng, M. D. Collins, Y. Zhu, T. Liu, T. S. Huang, H. Adam, and L.-C. Chen, "Panoptic-deeplab: A simple, strong, and fast baseline for bottom-up panoptic segmentation," in *Proceedings of the IEEE/CVF conference on computer vision and pattern recognition*, 2020, pp. 12 475–12 485.
- [27] B. Cheng, A. Schwing, and A. Kirillov, "Per-pixel classification is not all you need for semantic segmentation," *Advances in neural information processing systems*, vol. 34, pp. 17 864–17 875, 2021.
- [28] B. Cheng, I. Misra, A. G. Schwing, A. Kirillov, and R. Girdhar, "Masked-attention mask transformer for universal image segmentation," in *Proceedings of the IEEE/CVF conference on computer vision and pattern recognition*, 2022, pp. 1290–1299.
- [29] F. Li, H. Zhang, H. Xu, S. Liu, L. Zhang, L. M. Ni, and H.-Y. Shum, "Mask dino: Towards a unified transformer-based framework for object detection and segmentation," in *Proceedings of the IEEE/CVF Conference on Computer Vision and Pattern Recognition*, 2023, pp. 3041–3050.
- [30] J. Hu, L. Huang, T. Ren, S. Zhang, R. Ji, and L. Cao, "You only segment once: Towards real-time panoptic segmentation," in *Proceedings of the IEEE/CVF Conference on Computer Vision and Pattern Recognition*, 2023, pp. 17 819–17 829.
- [31] Z. Li, W. Wang, E. Xie, Z. Yu, A. Anandkumar, J. M. Alvarez, P. Luo, and T. Lu, "Panoptic segformer: Delving deeper into panoptic segmentation with transformers," in *Proceedings of the IEEE/CVF conference on computer vision and pattern recognition*, 2022, pp. 1280–1289.
- [32] J. Jain, J. Li, M. T. Chiu, A. Hassani, N. Orlov, and H. Shi, "Oneformer: One transformer to rule universal image segmentation," in *Proceedings of the IEEE/CVF Conference on Computer Vision and Pattern Recognition*, 2023, pp. 2989–2998.
- [33] A. Kortylewski, Q. Liu, A. Wang, Y. Sun, and A. Yuille, "Compositional convolutional neural networks: A robust and interpretable model for object recognition under occlusion," *International Journal of Computer Vision*, vol. 129, pp. 736–760, 2021.
- [34] X. Yuan, A. Kortylewski, Y. Sun, and A. Yuille, "Robust instance segmentation through reasoning about multi-object occlusion," in *Proceedings of the IEEE/CVF Conference on Computer Vision and Pattern Recognition*, 2021, pp. 11 141–11 150.
- [35] Y.-T. Chen, X. Liu, and M.-H. Yang, "Multi-instance object segmentation with occlusion handling," in *Proceedings of the IEEE Conference on Computer Vision and Pattern Recognition*, 2015, pp. 3470–3478.
- [36] G. Zhan, W. Xie, and A. Zisserman, "A tri-layer plugin to improve occluded detection," *arXiv preprint arXiv:2210.10046*, 2022.
- [37] L. Ke, Y.-W. Tai, and C.-K. Tang, "Deep occlusion-aware instance segmentation with overlapping bilayers," in *Proceedings of the IEEE/CVF conference on computer vision and pattern recognition*, 2021, pp. 4019–4028.
- [38] J. Qi, Y. Gao, Y. Hu, X. Wang, X. Liu, X. Bai, S. Belongie, A. Yuille, P. H. Torr, and S. Bai, "Occluded video instance segmentation: A benchmark," *International Journal of Computer Vision*, vol. 130, no. 8, pp. 2022–2039, 2022.
- [39] L. Yang, Y. Fan, and N. Xu, "Video instance segmentation," in *Proceedings of the IEEE/CVF International Conference on Computer Vision*, 2019, pp. 5188–5197.
- [40] H. Ding, C. Liu, S. He, X. Jiang, P. H. Torr, and S. Bai, "Mose: A new dataset for video object segmentation in complex scenes," *arXiv preprint arXiv:2302.01872*, 2023.
- [41] S. E. Palmer, *Vision science: Photons to phenomenology*. MIT press, 1999.